HEAT TRANSFER ENHANCEMENT USING PIEZOELECTRIC FAN IN ELECTRONIC COOLING - EXPERIMENTAL AND NUMERICAL OBSERVATIONS

M. K. ABDULLAH[*], B. H. MURNI, M. Z. ABDULLAH, M. A. MUJEEBU, F. HUSSIN, H. YUSOFF, N.C. ISMAIL, K. A. AHMAD AND Z. MOHD RIPIN

Aerodynamics and Advanced Cooling Laboratory, School of Mechanical and Aerospace Engineering,
Engineering Campus, Universiti Sains Malaysia
14300 Nibong Tebal, Penang, Malaysia, mkhalil@eng.usm.my

Abstract: Piezoelectric fan is an innovative design and feasible solution to remove heat from microelectronic systems for portable electronic products. It is small in size, has low power consumption and minimal noise. This paper presents experimental and computational investigations of incompressible three-dimensional streaming flows induced by piezoelectric fan and the associated heat transfer enhancement, on a Plastic Leaded Chip Carrier (PLCC) package. Piezoelectric fan (piezofan) is arranged at two different heights normal to the heat source surface (in each case, the normalized gap $\delta = G/l_p$) and tested for its performance, compared to the base case (natural convection or no fan). The flow field is observed and captured by means of a particle image velocimetry (PIV) system. The heat transfer coefficient in each case is also computed. The finite volume based computational fluid dynamics package, FLUENT 6.3.2 is used to investigate the heat transfer coefficient and the flow fields using a dynamic mesh option. The result shows that the piezofan yields significant improvement in heat transfer, and a normalized gap of 0.106 is offered a better cooling compared to the 0.0604. The experimental results are in good agreement with the predicted results.
Keywords: Electronic cooling, PLCC, Piezofan, Heat transfer coefficient.

ELEKTRONİK CİHAZ SOĞUTMADA PİEZOELEKTRİK FAN KULLANIMININ ISI TRANSFERİNİN İYİLEŞTİRİLMESİ – DENEYSEL VE SAYISAL GÖZLEMLER

Özet: Piezoelektrik fan taşınabilir elektronik ürünlerde ısının uzaklaştırılması için yernilikçi bir tasarım ve uygun bir çözümdür. Boyutları küçük, düşük güç tüketimi ve düşük gürültü seviyesine sahiptir. Bu makalede piezoelektrik fan tarafından hareketlendirilen sıkıştırlamaz üç boyutlu akış ve ısı transferi bir Plastik Leaded Yonga Taşıyıcı (PLCC) paketi incelenmiş ve sunulmuştur. Piezoelektrik fan (piezofan) ısı kaynağı yüzeyine dik olarak iki farklı yükseklikte konumlandırılmış (her bir durum için, normalize edilmiş aralık $\delta = G/l_p$) ve performansı test edilmiş, temel durum (doğal taşınım veya fansız durum) ile kıyaslanmıştır. Akış alanı, parçacık görüntülemeli hız ölçer (PIV) sistemi aracılığıyla gözlenmiş ve ölçülmüştür. Her durum için ısı transfer katsayısı da hesaplanmıştır. Sonlu hacimler yöntemi tabanlı hesaplamalı akışkanlar dinamiği programı FLUENT 6.3.2 dinamik ağ seçeneği kullanılarak ısı transferi ve akış alanları incelenmiştir. Sonuç, piezofanın ısı transferini önemli ölçüde iyileştirdiğini, ve 0,106 olan normalize edilmiş aralığın 0.0604 değerinden daha iyi soğuttuğunu göstermiştir. Deneysel sonuçlar sayısal sonuçlarla uyum içerisindedirler.
Anahtar Kelimeler: Electronik soğutma, PLCC, Piezofan, Isı transferi katsayısı.

NOMENCLATURE

A	Frequency dependent amplitude
A_h	Area of heater surface (m^2)
F	Body force (m/s^2)
g	Gravitational acceleration (m/s^2)
G	Height of piezofan from heat source (m)
H	Height of test section (m)
h	Static enthalpy (j/kg)
h_{ave}	Average of convection coefficient (W/m^2K)
h_{hor}	Length of resolution
k	Fluid thermal conductivity (W/mK)
L	Length of test section (m)
l_p	Length of piezofan (m)
l_u	Length of piezofan without PZT patch (m)
P	Pressure (Pa)
t	Time (s)
t_p	Piezofan thickness (m)
Q	Heater power (W)
S	Source term
T	Temperature (K)
T_h	Heater temperature (K)
T_a	Ambient temperature (K)
u, v, w	Velocity component (m/s)
$\vec{u}$	Velocity vector
u_g	Grid velocity

V	Control volume	τ	Shear stress (N/m^2)
v_{ver}	Height of resolution	β	Eigen value
W	Width of test section (m)	*Subscripts*	
w	Blade position (m)	a	Ambient
$\dot{w}$	Blade velocity (rad/s)	ave	Average
w_P	Width of piezofan (m)	g	Grid
x, y, z	Space coordinates	h	Heater
Greek symbols		hor	Horizontal
Γ	Diffusion coefficient	i, j, k	Coordinate indices
ρ	Fluid density (kg/m^3)	p	Piezofan
ω	Angular velocity (rad/s)	ver	Vertical
δ	Normalized gap		
Φ	General scalar for transport equation		

INTRODUCTION

The continuing increase of power densities in microelectronics and simultaneous drive to reduce the size and weight of electronic products have led to crucial thermal management issues in the industry. Inappropriate thermal management of the electronic device degrades its performance significantly (Sparrow *et al.*, 1982). The conventional cooling devices such as rotary fan and heat sink are popular in the current market. Ironically, they are not so suitable for portable devices such as laptop and mobile phone owing to space and power limitations (Sparrow *et al.*, 1983). Plastic Leaded Chip Carrier (PLCC) arrangement is an alternative that can be used in portable electronic devices to improve thermal performance and hence the electronic performance (Mohamed *et al.*, 2008). However, a PLCC alone cannot resolve the issue since it also requires a cooling mechanism. One of the viable solutions is piezoelectric fan, hereafter named as piezofan. It is an innovative design which is gaining acceptance as feasible solution for portable electronic products (Buermann *et al.*, 2002). Piezofan generally consists of a patch of piezoelectric material bonded to a flexible cantilever blade. An alternating voltage is applied to the piezoelectric patch; it expands and contracts in the lengthwise direction, causing bending moments at both ends of the patch. These moments drive the attached blade to oscillate at the same frequency (Kim *et al.*, 2005). These piezofans use very little power and can be developed to meet various geometric constraints for many applications (Kimber and Garimella, 2009). It clearly enhances the heat transfer when compared to natural convection. This technology is desirable because it is noiseless at the frequencies of operation, compact, light in weight and durable (Garimella *et al.*, 2006). A number of studies on piezofan were reported in the literature. Toda and Osaka (1979 &1981) found that placing a piezoelectric fan on either side of a power transistor panel of a television receiver resulted in temperature reductions of 17°C and 5°C on the panel surface and inner space respectively. A numerical model was developed by Acikalin and Garimella (2009), to analyze the operation of a piezoelectrically actuated cantilever vibrating close to a heated surface. They found that the length as well as the frequency of the piezofan could alter its heat

transfer characteristics. Yoo *et al.* (2000) fabricated various kinds of piezofans and characterized the induced flow for application to electronic cooling apparatus. It was found that the most effective fan was the one made from a phosphor bronze shim and with PZT in a bimorph configuration where it shows a tip displacement of 35.5 mm and a produced wind velocity of 3.1 m/s driven by a 220 V, 60 Hz power source. Kwon *et al.* (2005) studied the vibration characteristic of piezoelectric vibration actuator. The geometric size of the vibration device has decided the resonance frequency dependency according to the change of length, width, thickness and dummy weight of the vibration device where energy conversion efficiency could become the maximum. The performance of piezofan operating at higher resonance modes was studied in detail by Wait *et al.* (2007) who showed that certain advantages of piezofan operation at higher resonance modes were offset by increased power consumption and decreased fluid flow. Abdullah *et al.* (2008, 2009) investigated the effect of piezofan height on the performance of piezofan both numerically and experimentally. They found that, the heat transfer coefficient was significantly affected by the height of piezofan from the heat source. The piezofan swinging was observed to be an unsteady phenomenon and influenced the flow behavior on the heat source surface. Liu *et al.* (2009) studied the influence of horizontal and vertical arrangements of piezofans, and found that the heat transfer augmentation of the piezofan was resulted from the entrained airflow during each oscillation cycle, and the jet-like air stream at the fan tip. The heat transfer performance for vertical arrangement showed a symmetrical distribution and peaked at the center region whereas the horizontal arrangement possessed an asymmetrical distribution and showed an early peak at $x/L = 0.25$. It was also found that the heat transfer performance for horizontal arrangement was not necessarily lower than that of vertical one. In the current study, the potential offered by piezofan for the thermal management of PLCC package is assessed experimentally as well as numerically. As far as the authors are aware, the previous works focused only on two-dimensional simulations, owing to the complexity of displacement of the vibrating blade and the computer-intensive nature of the numerical model. In the present study, a three-dimensional modeling is performed using FLUENT 6.3., in order to have more

realistic analysis of fluid and temperature fields during piezofan operation. Two different experimental configurations are set up in order to study the effect of piezofans on the heat transfer from a small, vertically mounted heat source which duplicates the PLCC. Experiments are conducted for two different gaps of piezofan, and the results are compared with the base case (no fan condition). Particle image velocimetry (PIV) technique is used to make the flow measurements.

EXPERIMENTAL APPARATUS AND PROCEDURE

The flow visualization experiments are conducted to gain insight into the flow induced by the piezofan. The schematic of experimental setup used in the present study is shown in Figure 1. A clear glass tunnel of size 0.25m (H) × 0.06m (W) × 0.8m (L) is constructed to act as the test section. The electronic chip (PLCC) is replicated as a heater with constant heat flux of 4.6 kW/m^2 controlled by a direct current (DC) power supply (GW instek GPS2303). The stainless steel heater of dimension 0.03m × 0.03m × 0.003m, is embedded onto a wooden platform which also serves as thermal insulator. The heater along with the piezofan is housed by the glass tunnel. The heater and ambient air temperatures are measured at one minute interval, by thermocouples linked to computer by means of a data logger (ADVANTECH DAQ System). Table 1 summarizes the specifications of the piezofan which is arranged vertically at two different normalized gaps (δ) defined by, $\delta = G/l_p$ (G and l_p are shown in Figure 2). The piezofan is operated in the first mode condition and excited at its resonance in order to achieve the maximum vibration amplitude. DC to AC inverter circuit (Kit inverter) is used to facilitate oscillating drive signal according to the resonance frequency of the piezofan; the applied voltage and resonance frequency are measured by an oscilloscope (Agilent Technologies DSO3062-60MHz). Seeding for the PIV system is facilitated by atomized corn oil particles slowly drawn into the glass tunnel. The air flow is supplied by a reciprocating air compressor, and regulated by an air flow-meter. The nominal diameter of the corn oil particle is 1 to 2 μm in size (Melling, 1997). The leading edge of the wooden platform is made inclined at an angle 45° in order to avoid the flow separation. A Dantec 2D particle image velocimetry (PIV) system has been used to measure the velocity induced by the piezofan. The CCD camera in conjunction with a double pulse Nd: YAG laser captures the flow field induced by the piezofan and the images are stored in the computer via a PIV controller unit. A section of the flow was illuminated with long exposure with light sheet generated by a 300mW Argon-ion laser and the beam reflected 90° by a mirror and the narrow sheet of

Table 1. Specifications of the piezofan (Piezo Systems Inc., USA).

Specification	Value
Material	Stainless steel
Piezofan size (m)	0.047 (l_P) × 0.012 (w_P) × 0.0004 (t_P)
Piezofan height without patch (m)	0.023 (l_u)
Resonant frequency (Hz)	115
Power consumption of piezofan and circuit (mW)	42
Blade swing, peak to peak (m)	0.0098
Piezofan weight (kg)	0.002
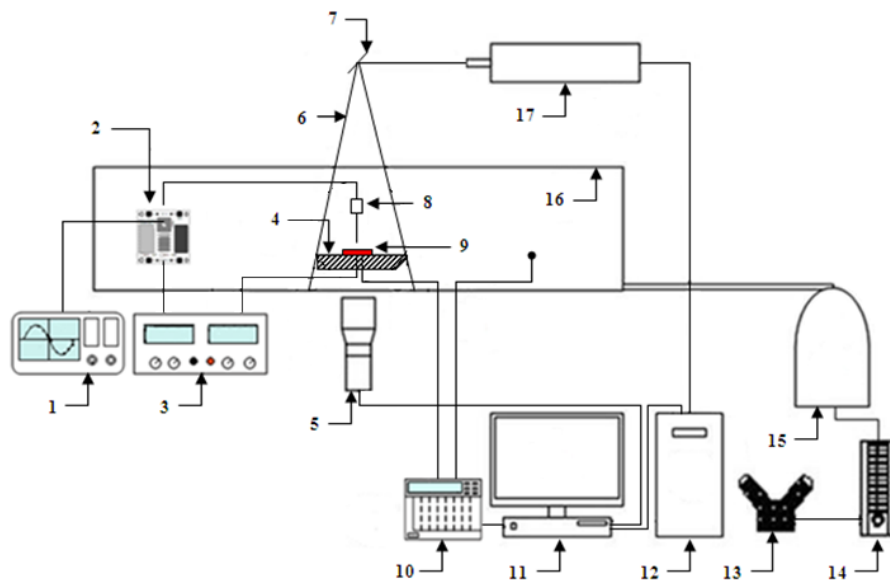
1	Oscilloscope	7	Mirror		13	Air compressor
2	Kit inverter	8	Piezofan	14		Air controller
3	Dual digital power supply	9	Heater		15	Atomizer
4	Wood platform	10	Temperature DAQ	16		Glass tunnel
5	CCD camera	11	Personal computer	17		Laser
6	Laser sheet	12	Laser controller			

Figure 1. Schematic of the experimental setup.

light that is produced through the convex lens and cylindrical lens. The thickness of the laser sheet illuminating the flow field was approximately 1.0 mm. A digital video camera (Digital monochrome progressive scan camera; Flowsense M2 8bits) with a resolution of 1600 (h_{hor}) × 1186 (v_{ver}) pixels was used to record of two sequence of frame continuously with 4μ second for each frame. Live feedback of the images was displayed on a screen monitor connected to the video camera. Selected scene or sequence images were stored in the computer by using FlowManager™ software. It also offered two-frame cross-correlation technique to calculate the raw displacement vector field from the particle image velocity data. In the image processing, 64 × 64 pixels rectangular effective interrogation windows were used. Velocity vectors of the flow were calculated from this displacement vector field.
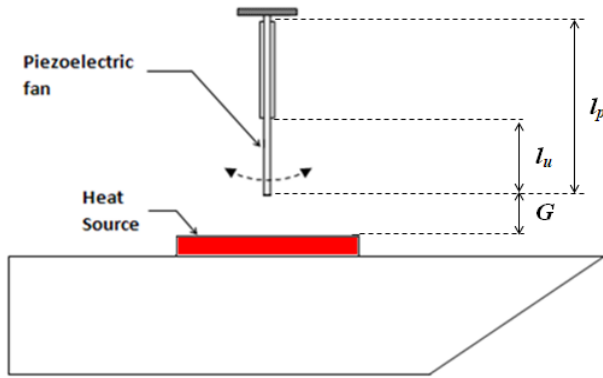
Figure 2. Illustration of gap G, piezofan height l_p, and un-patched length of piezofan l_u.

SIMULATION SETUP

The physical model for simulation is in accordance with the experimental setup (but size is reduced to one third), which contains the glass tunnel, heater, wood platform and piezofan as shown in Figure 3. The four sides of the enclosure and wood platform are set as isothermal walls in the numerical model. A uniform heat flux of 4.6 kW/m^2 is imposed as the heat source. The left and right boundaries are set as pressure outlets, and the clamp of the piezofan is neglected. The blade (piezofan) swinging phenomena is set to move according to the simple harmonic vibration equations (5) – (8) and its position is calculated accordingly, at each time step. This boundary is modeled as a moving adiabatic wall whose location in time is set by a user-defined function (UDF) in C language, with no thermal conduction allowed through it.

The hybrid elements are used in the present 3-D analysis. The flow is assumed as laminar and incompressible with no radiation contributions. First-order upwind discretization is used both for momentum and energy, and the SIMPLE scheme is used for pressure-velocity coupling. The convergence factors have been set to 1×10^{-3} and 1×10^{-6} for continuity and momentum, and energy respectively. The piezofan is set to vibrate at 115Hz corresponding to a period approximately 0.0087s for each case. The heat transfer

coefficient based on the average fluid and heat source surface temperatures is calculated. The total duration of the simulation is selected such that the heat transfer coefficient has reached a steady value during this period. This took 150,000 time steps, which corresponds to approximately 4 days of computation time per each case on a Pentium Quadcore processor (2.8 GHz) computer with 2 GB of memory. The effects of time step and mesh size are investigated to verify that the solution is independent of those parameters. Time-step size of 0.0001s is chosen for all the cases to achieve numerical stability, with the mesh size around 180,000 elements (87 time steps per cycle of piezofan vibration). These values are arrived at after three attempts to check the trend and proximity with the profiles investigated. For instance, the trials are done by increasing the mesh elements and decreasing the time steps. However, a problem arose when the mesh elements were increased, due to the negative volume detected in FLUENT during analysis. This problem is typically found in dynamic meshing setup.

1 Pressure outlet-1	4 Bottom wall	7 Left wall
2 Heater	5 Top wall	8 Pressure outlet-2
3 Wood platform	6 Piezofan	9 Right wall
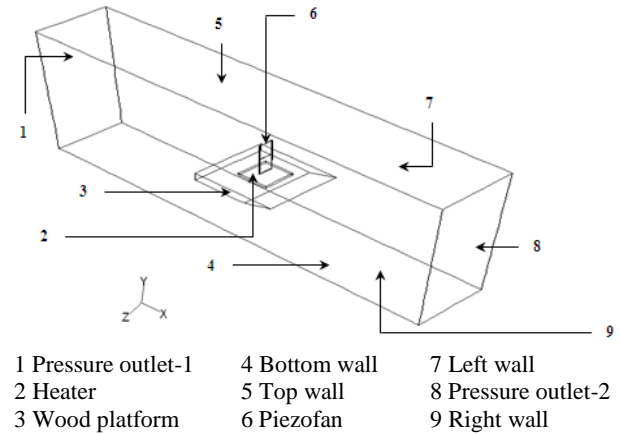
Figure 3. 3-D view of the simulation set-up.

NUMERICAL MODEL

The flow is assumed as laminar and incompressible with no radiation contribution. The governing equations are chosen accordingly (FLUENT©, 2006) along with the necessary boundary conditions of the flow domain, as follows.

The conservation of mass is:

$$\frac{\partial \rho}{\partial t} + \frac{\partial}{\partial x_i}(\rho u_i) = 0 \qquad (1)$$

The conservation of momentum in i-th direction in an inertial (non-accelerating) reference frame is described by:

$$\frac{\partial}{\partial t}(\rho u_i) + \frac{\partial}{\partial x_j}(\rho u_i u_j) = -\frac{\partial P}{\partial x_i} + \frac{\partial \tau_{ij}}{\partial x_j} \qquad (2)$$

where, P is the static pressure, and τ_{ij} is the viscous stress tensor.

44

The energy equation in terms of h (static enthalpy) can be written as,

$$\frac{\partial}{\partial t}(\rho h) + \frac{\partial}{\partial x_i}(\rho u_i h) = \frac{\partial}{\partial x_j}(k\frac{\partial T}{\partial x_i}) \quad (3)$$

where T is the temperature and k is the thermal conductivity.

The integral form of the transport equation for a general scalar, Φ on an arbitrary control volume, V, on a moving mesh is written as,

$$\frac{d}{dt}\int_V \rho\Phi dV + \int_{\partial V}\rho\Phi(\vec{u}-\vec{u}_g)dA = \int_{\partial V}\Gamma\nabla\Phi dA + \int_V S_\Phi dV \quad (4)$$

where $\vec{u}$ is the flow velocity vector and $\vec{u}_g$ is the grid velocity of the moving meshes. The first and second terms on the left are the time derivative term and the convective term respectively. The terms on the right are the diffusive and the source terms. The term Γ represents the diffusion coefficient and S_Φ represents the source term of Φ. The term ∂V represents the boundary of the control volume V and dA is the area movement.

The resulting mode shapes of a piezofan can be approximated by the mode shape of a clamped-free blade. Assuming a sinusoidal driving, position of the blade is given by Meirovitch (1997):

$$w(x,t) = A \cdot \left[\begin{array}{l} (\sin(\beta l_u)-\sinh(\beta l_u))(\sin(\beta x)-\sinh(\beta x)) \\ +(\cos(\beta l_u)+\cosh(\beta l_u))(\cos(\beta x)-\cosh(\beta x)) \end{array} \right] \cdot \sin(\omega t) \quad (5)$$

Differentiating this equation with respect to time gives the velocity of the blade,

$$\dot{w}(x,t) = A \cdot \left[\begin{array}{l} (\sin(\beta l_u)-\sinh(\beta l_u))(\sin(\beta x)-\sinh(\beta x)) \\ +(\cos(\beta l_u)+\cosh(\beta l_u))(\cos(\beta x)-\cosh(\beta x)) \end{array} \right] \cdot \omega\cos(\omega t) \quad (6)$$

Where β values can be calculated from the frequency equation

$$\cos(\beta l_u) \cdot \cosh(\beta l_u) = -1 \quad (7)$$

This must be solved numerically and yields infinity solutions of β. The β value corresponding to the first mode shape is

$$\beta = \frac{1.875}{l_u} \quad (8)$$

All surfaces of the enclosure, the platform, and the heat source surfaces, are identified as no-slip boundary conditions. Figure 4 shows the position of the blade with respect to the phase angle (product of angular velocity and time) for 0.0049m peak to peak deflection. Figure 5 shows the velocity of the blade at different positions (x) with respect to time, in one cycle.
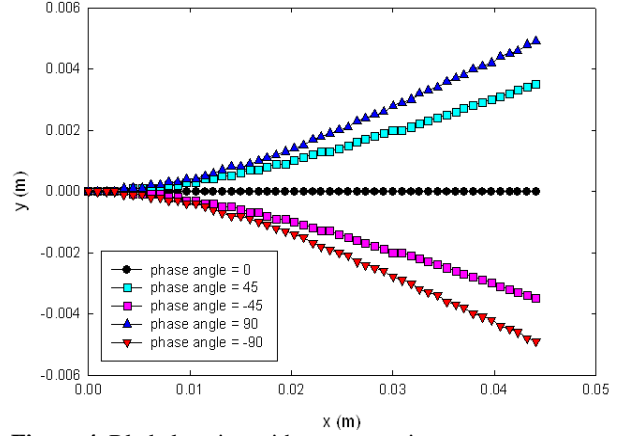
Figure 4. Blade location with respect to time.
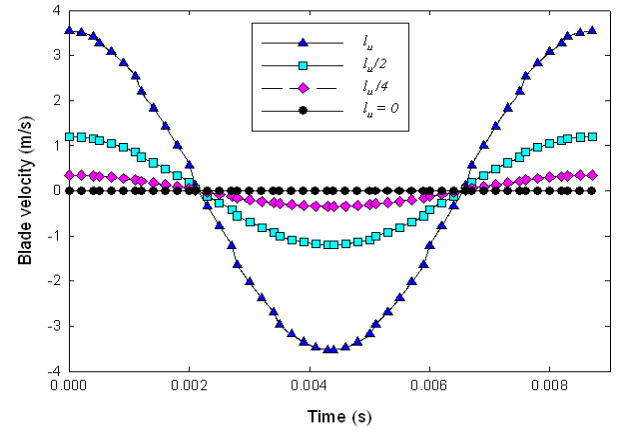
Figure 5. Blade velocity at different positions of blade.

RESULTS AND DISCUSSION

Flow Profiles And Velocity Vectors

The goal of this study is to analyze the flow and heat transfer enhancement by using piezofan at for two different normalized gaps, $\delta = 0.064$ and $\delta = 0.106$. Figure 6 shows the transient flow generated by the piezofan at $\delta = 0.106$. Creation of vortices due to piezofan deflection is visualized by the oil smoke particles. The results clearly show the development of vortices according to the swinging of the piezofan. When the piezofan swings left, the vortex is observed at the left side and when swings right, the left side vortex slowly disappears and emerges at the right side of the piezofan. Double vortices are developed on both the sides after the piezofan is moved to the neutral position.

Figure 7 shows the velocity vectors for $\delta = 0.0604$, measured at two different times i.e., when the piezofan swings towards right (Figure 7a) and left (Figure 7b). The piezofan is first adjusted to the resonance mode but when it operates the velocity is induced very much depending on its direction of movement. It is observed that more velocity is induced when the piezofan swings towards left, as evidenced by a higher volume of flow on the PLCC surface where the maximum velocity reaches about 1.5m/s. As the piezofan swings right less

45
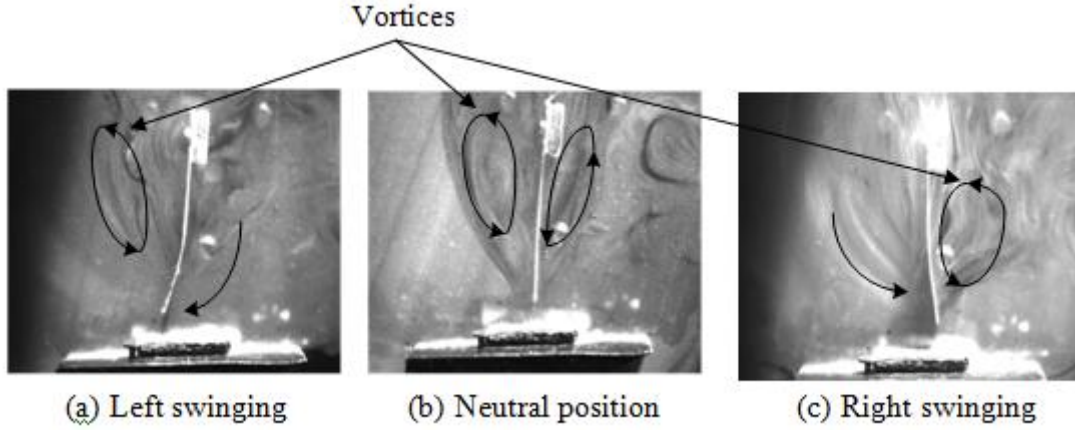
Figure 6. Vortex formations at different swinging positions of the piezofan (for δ = 0.106).

volume of flow is observed, with the velocity reaching to a maximum of 1.0m/s.

Figure 8a and Figure 8b respectively show the velocity vectors for right and left swinging when the piezofan is located at δ = 0.106. The velocity vectors of higher magnitude are induced on the top surface of the heat source where the maximum velocity reaches up to 2.0m/s especially when the piezofan swings towards left. For the rightward swing, the velocity is slightly lowered to about 1.7m/s. It is obvious that, as δ increases the induced volume of flow also increases which provide better convective heat transfer.

Figure 9 shows the velocity vectors when the piezofan is located at δ = 0.064. The vectors are observed at three different piezofan positions namely initial (Figure 9a), left swing (Figure 9b) and right swing (Figure 9c). Two regions of circulation are observed on either side of the vibrating piezofan, owing to its rapid swinging. The maximum velocity when the piezofan swings left is found to be1.52m/s and for right swing, it is 1.1m/s.

Figures 10a to 10c illustrate the velocity vectors for three different time intervals at δ = 0.106. Here also, the results show that the velocity vector induced depends on the piezofan swinging. The induced velocity is higher when the piezofan swings left/rightwards on the PLCC surface. The double vortex generated by the induced flow using a piezofan is observed and the vortex moved downward to heat source surface. The maximum velocities during leftward and right ward swings are observed to be 2.05m/s and 1.75m/s respectively. In both the cases, the predicted velocities closely match the experimental results. Figure 11 shows the comparison of predicted and experimental results of velocities during right and left swings of the piezofan and heat transfer coefficient, for 0.064 and 0.106.

Heat Transfer Coefficient

At first, the temperature of the PLCC under natural convection (piezofan turned off) is set-up with a heat flux of 4.6kW/m^2 and maintained the same in all the experiments, without overheating the heat source.

Whenever the temperatures in the heater showed no variation over a period (at t = 1800s), it was assumed that steady-state operating conditions had been reached and it found to be 110°C. The heat transfer coefficient, h_{ave} is defined by using an energy balance between the power input and the heat removed from the surface of the heat source by convection, according to:

$$h_{ave} = \frac{Q}{A_h(T_h - T_a)} \quad (9)$$

where q is the power input to the heat source, A_h is the exposed surface area of the heater block. T_a is
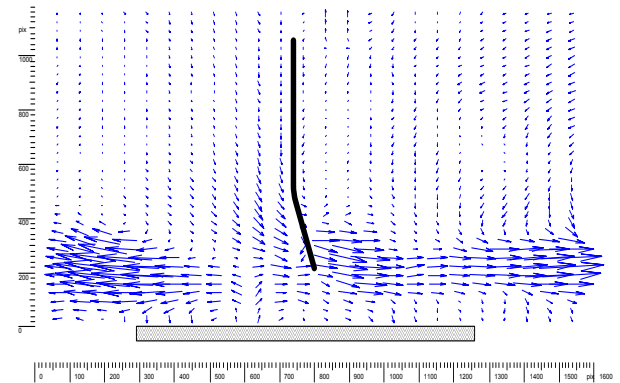
Figure 7a. Velocity vectors when piezofan swings right, at δ = 0.064
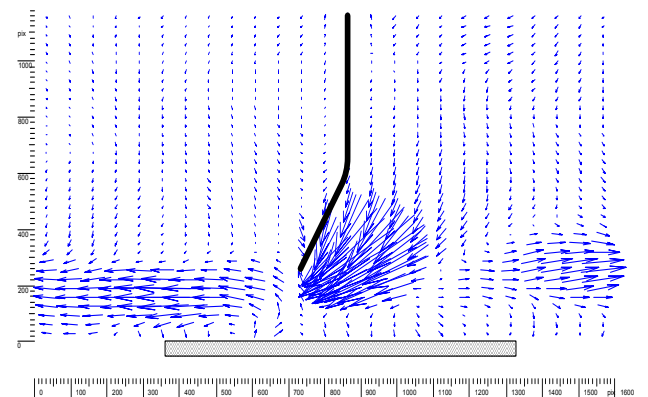
Figure 7b. Velocity vectors when piezofan swings left, at δ = 0.064.
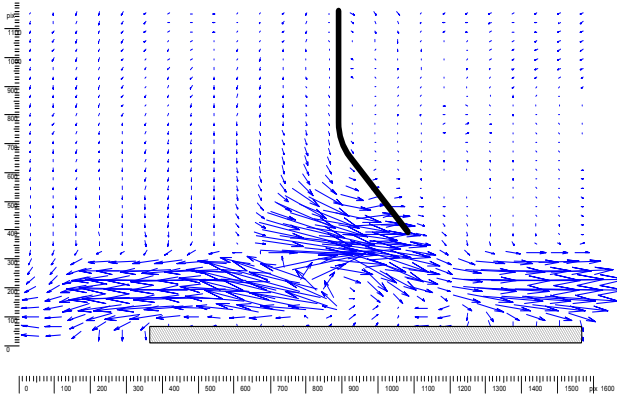
Figure 8a. Velocity vectors when piezofan swings right, at δ = 0.106.
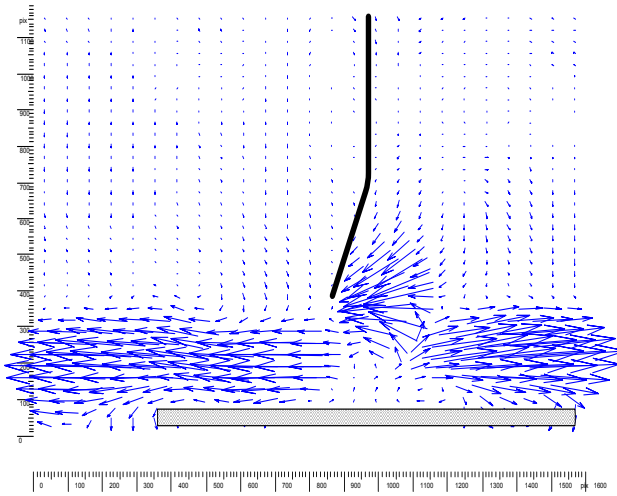
Figure 8b. Velocity vectors when piezofan swings left, at δ = 0.106.

the temperatures from thermocouples used to measure the air temperature over the test section at different locations. Another thermocouple was used to monitor the temperature of the heat source (T_h).

The piezofan is then turned on at $t = 3600$s and the system was allowed to reach new steady-state temperatures for the heat source and surrounding air at the same input power, and the new heat transfer coefficient was calculated. The new steady state is reached at $t = 5100$s, for both the cases. The piezofan is seen to cause a reduction in the heat source temperature from 110°C to 80°C and 60°C for δ = 0.064 and δ = 0.106 respectively. The temperature drop for the two different piezoelectric piezofan gap studied are plotted in Figure 12. It is apparent that the heat removal rate is maximum at δ = 0.106, where there is 168% increase in the heat transfer coefficient, relative to the base case; for δ = 0.064, it is limited to only 61%. This is because, at δ = 0.106, the piezofan provides more air flow around the PLCC, compared to δ = 0.064.

Figure 13 shows the temperature contours at different piezofan positions for δ = 0.064 and 0.106 respectively. The heat from the heat source surface is slowly removed by the air flow that is induced by the piezofan. The temperature on the heat source decreases gradually since the piezoelectric piezofan is operating. It is presumed the heat convection has reached the steady state condition whenever the temperature gradient has no change with the time step. The contours dictate that the piezofan reduces the temperature on the PLCC. The temperatures are observed to be 84°C and 63°C for δ = 0.064 and 0.106 respectively. The predicted heat transfer coefficients are 49% for δ = 0.064 and 146% for δ = 0.106. Lack of symmetry in contours about the main axis are observed, which may be attributed to the use of unstructured mesh

| | | |
| (a) Initial | (b) Left swing | (c) Right swing |
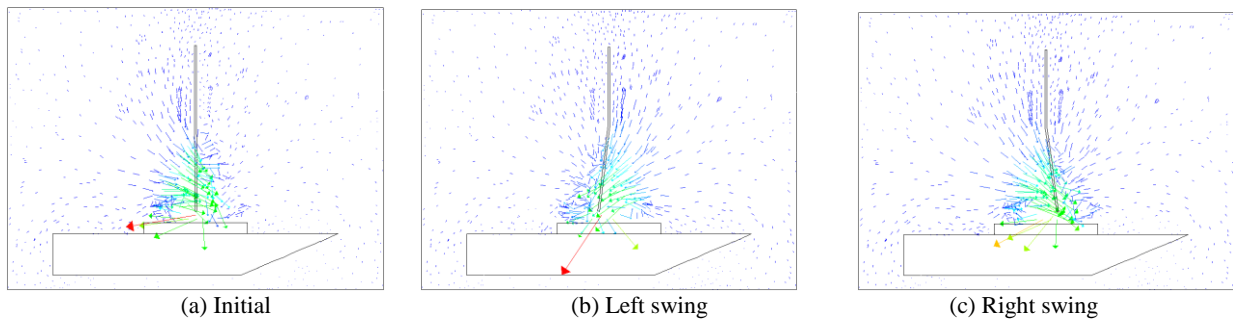
Figure 9. Velocity vector for δ = 0.064 at different piezofan positions.

| | | |
| (a) Initial | (b) Left swing | (c) Right swing |
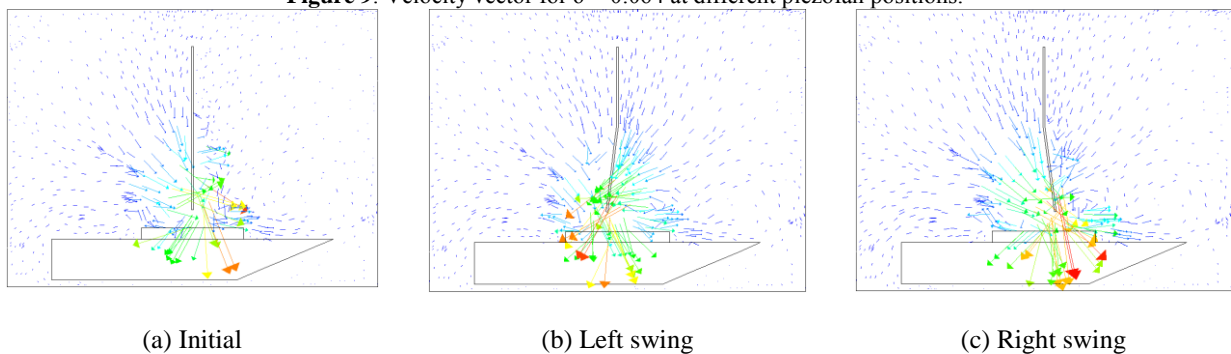
Figure 10. Velocity vector for δ = 0.106 at different time intervals.

which is chosen to facilitate the dynamic meshing. Figure 14 shows the comparison of predicted and experimental heat transfer coefficients for $\delta = 0.064$ and $\delta = 0.106$. The predictions are in good agreement with the experimental results (discrepancy is within 10%).
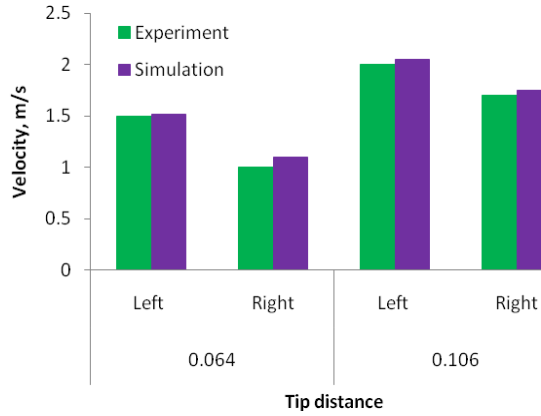
Figure 11. Comparison of the computed maximum velocity with the experimental flow visualization
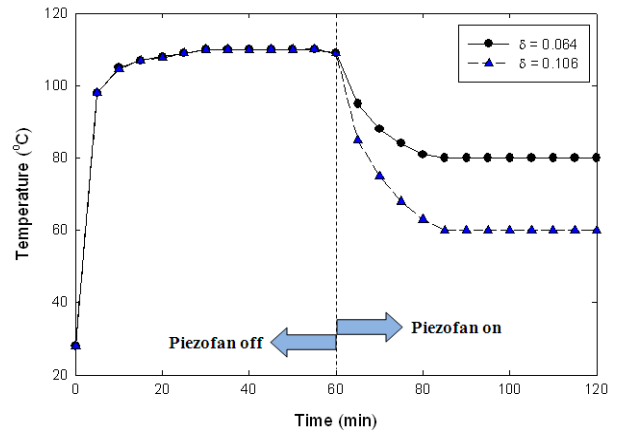
Figure 12. Effect of non-dimensional gap, δ on PLCC surface temperature.

(a) 0.064   **(b) 0.106**
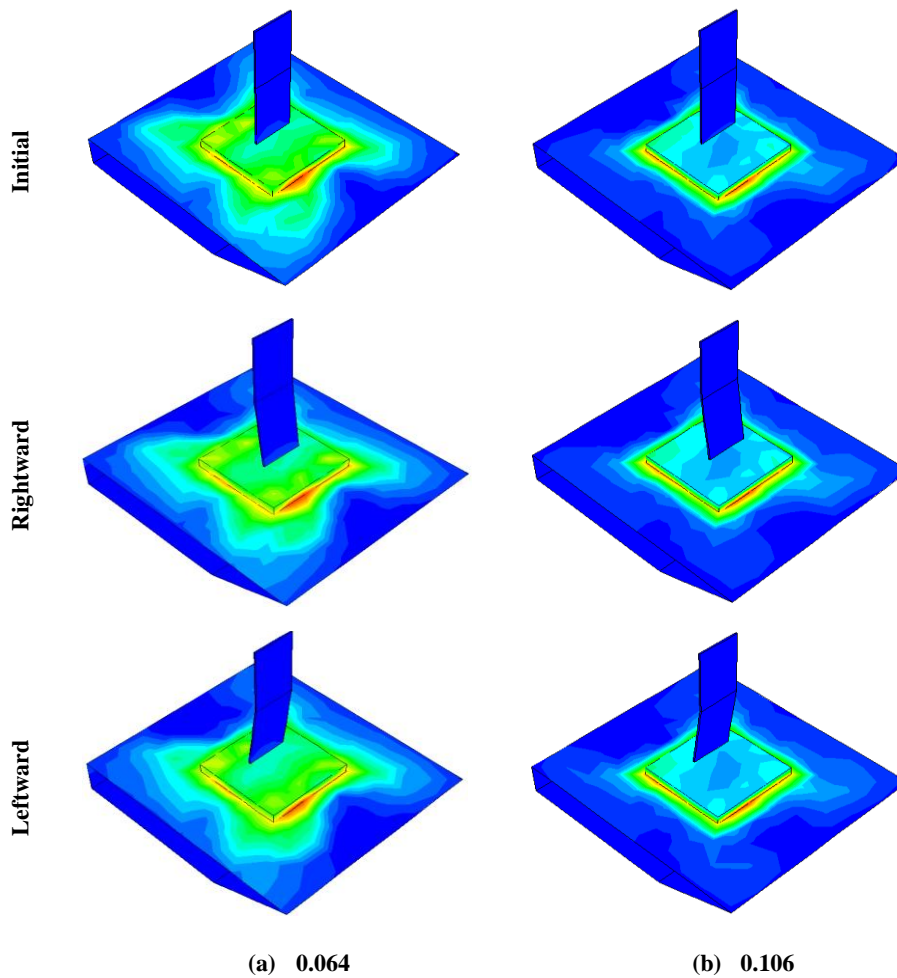
Figure 13. Temperature contours for (a) $\delta = 0.064$ and (b) $\delta = 0.106$ at three different positions.
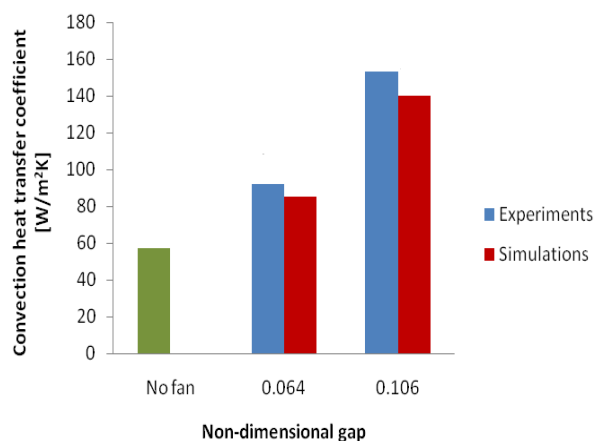
Figure 14. Comparison of predicted and experimentally determined heat transfer coefficients

CONCLUSION

Experimental investigation and three dimensional numerical simulations are performed for a piezofan for two different gaps, and the thermal performance is compared with the base case (no fan). In numerical modeling, utmost care is exercised to emulate the realistic situation of a PLCC package. The piezofan operation is modeled using the dynamic meshes in FLUENT 6.3 software and the induced flow and heat convection involved are predicted. The piezofan swinging is observed to be of unsteady nature, which influenced the flow behavior on the PLCC surface. A gap of $\delta = 0.106$ yielded better heat transfer coefficient compared to the base case. The heat transfer coefficient predicted by CFD simulation also shown satisfactory agreement with the experimental data with a difference of 10%. Therefore, piezofan has shown to be a viable solution for the thermal management of PLCC packages. Similar experiments may be carried out for different gaps to arrive at the optimum gap, for various orientations of piezofan, and for more number of PLCC packages. The effect of enclosure for miniaturized systems is very crucial; so this issue may also be incorporated in future works.

REFERENCES

Abdullah, M.K., Abdullah, M.Z., Ramana, M.V., Khor, C.Y., Ahmad, K.A., Mujeebu, M.A., Ooi, Y. and Mohd Ripin, Z., Numerical and Experimental Investigations on Effect of Fan Height on the Performance of Piezoelectric Fan in Microelectronic Cooling, *International Communications in Heat And Mass Transfer*, 36,51–58, 2009.

Abdullah, M.K., Abdullah M.Z., Ramana, M.V., Khor, C.Y., Ahmad, K.A., Mujeebu, M.A., Ooi, Y. and Mohd Ripin, Z., Effect of Piezoelectric Fan Height on Flow and Heat Transfer for Electronics Cooling Applications, *International Conference on Electronic Materials and Packaging, EMAP 2008*, Taipei, Taiwan, 165-170, 2008.

Acikalin, T. and Garimella, S.V., Analysis and Prediction of the Thermal Performance of Piezoelectrically Actuated Fans, *Heat Transfer Engineering*, 30(6), 487–498, 2009.

Acikalin, T., Wait, S.M., Basak, S., Garimella, S.V., Raman, A., Experimental Investigation of the Thermal Performance of Piezoelectric Fans, *Heat Transfer Engineering,* 25:4–14, 2004.

Buermann, P., Raman, A., Garimella, S.V., Dynamics and Topology Optimization of Piezoelectric Fans, *IEEE Transactions on Components and Packaging Technologies,* 25(4), 592-600, 2003.

FLUENT© user's manual, Retrieved September 20, 2006 from the World Wide Web: http://www.fluentusers.com/fluent63/doc/ori/index.htm Garimella, S.V., Advances in Mesoscale Thermal Management Technologies for Microelectronics, *Microelectronics Journal*, 37, 1165–1185, 2006.

Kim, B.J., Rho, J.S., and Jung, H.K., Optimal Design of Piezoelectric Cantilever Fan by Three-Dimensional Finite Element Analysis, *KIEE International Transaction on Electrical Machinery and Energy Conversion Systems*, 5-B(1), 90-94, 2005.

Kimber, M., Garimella, S.V. and Raman, A., An Experimental Study of Fluidic Coupling Between Multiple Piezoelectric Fans, *The Tenth Intersociety Conference on Thermal and Thermomechanical Phenomena in Electronics Systems, ITHERM 2006*, SanDiego, 333-340 2006.

Kimber, M., Suzuki, K., Kitsunai, N., Seki, K. and Garimella, S.V., Quantification of Piezoelectric Fan Flow Rate Performance and Experimental Identification of Installation Effects, *11th Intersociety Conference on Thermal and Thermomechanical Phenomena in Electronic Systems, ITHERM 2008*, Florida, 471-479. 2008.

Kimber, M. and Garimella, S.V., Measurement and prediction of the cooling characteristics of a generalized vibrating piezoelectric fan, *International Journal of Heat and Mass Transfer*, 52, 4470–4478, 2009.

Kwon, O.D., Yoo. J.S., Yun, Y.J., Lee, J.S., Kang. S.H. and Lim, K,J, A Research on the Piezoelectric Vibration Actuator for Mobile Phone, *Proceedings of International Symposium on Electrical Insulating Materials, ISEIM 2005*, Kitakyushu, Japan, 3, 676-678, 2005.

Liu, S.F., Huang, R.T., Sheu. W.J. and Wang, C.C., Heat Transfer by a Piezoelectric Fan on a Flat Surface Subject to the Influence of Horizontal/Vertical Arrangement, *International Journal of Heat and Mass Transfer*, 52,2565–2570, 2009.

Meirovitch, L., *Principals and techniques of Vibration*, Englewood Cliffs, Prentice Hall, 1997.

Melling, A., Tracer Particles and Seeding for Particle Image Velocimetry, *Meas. Sci. Technology*, 8, 1406–1416 1997.

Mohamed, M., Deraman, R., Abdullah, M.Z., Mujeebu, M.A., Abdullah, M.K., Three Dimensional CFD Simulation For 8 PLCC Packages Mounted Inline on a Printed Circuit Board, *Esteem*, 4, 1, 79-100, 2008 .

Sparrow, E.M., Niethammer, J.E. and Chaboki, A., Heat Transfer And Pressure Drop Characteristics of Arrays of Rectangular Modules Encountered in Electronic Equipment, *International Journal of Heat and Mass Transfer*, 25, 961-973, 1982.

Sparrow, E.M., Vemuri, S.B. and Kadle, D.S., Enhanced and Local Heat Transfer, Pressure Drop and Flow Visualization for Array of Block Like in Electronic Equipment, *International Journal of Heat and Mass Transfer*, 26(5),689-699, 1983.

Toda, M., Osaka, S., Vibrational Fan Using the Piezoelectric Polymer PVF$_2$, *Proceedings of the IEEE*, 67(8):1171-1173, 1979.

Toda, M., Voltage-induced Large Amplitude Bending Device-PVF Bimorph—Its Properties and Applications, *Ferroelectrics*, 32, 127– 133, 1981.

Wait, S.M., Basak, S., Garimella, S.V. and Raman, A., Piezoelectric Fans Using Higher Flexural Modes for Electronics Cooling Applications, *IEEE Transactions on Components and Packaging Technologies,* 30(1), 119-128, 2007.

Yoo, J.H., Hong, J.I. and Cao, W., Piezoelectric Ceramic Bimorph Coupled to Thin Metal Plate as Cooling Fan for Electronic Devices, *Sensors And Actuators A*, 79, 8–12, 2000.